Forty-five degree backscattering-mode nonlinear absorption imaging in turbid media

Liping Cui
Wayne H. Knox
University of Rochester
The Institute of Optics
275 Hutchinson Road
Rochester, New York 14627

Abstract. Two-color nonlinear absorption imaging has been previously demonstrated with endogenous contrast of hemoglobin and melanin in turbid media using transmission-mode detection and a dual-laser technology approach. For clinical applications, it would be generally preferable to use backscattering mode detection and a simpler single-laser technology. We demonstrate that imaging in backscattering mode in turbid media using nonlinear absorption can be obtained with as little as 1-mW average power per beam with a single laser source. Images have been achieved with a detector receiving backscattered light at a 45-deg angle relative to the incoming beams' direction. We obtain images of capillary tube phantoms with resolution as high as 20 μm and penetration depth up to 0.9 mm for a 300-μm tube at SNR ~1 in calibrated scattering solutions. Simulation results of the backscattering and detection process using nonimaging optics are demonstrated. A Monte Carlo–based method shows that the nonlinear signal drops exponentially as the depth increases, which agrees well with our experimental results. Simulation also shows that with our current detection method, only 2% of the signal is typically collected with a 5-mm-radius detector. [DOI: 10.1117/1.3368995]

Keywords: nonlinear absorption; multiphoton microscopy; turbid media; epi-mode; Monte Carlo.

Paper 09392R received Sep. 2, 2009; revised manuscript received Dec. 7, 2009; accepted for publication Jan. 15, 2010; published online Mar. 23, 2010.

1 Introduction

Nonlinear optical imaging is based on a nonlinear light–matter interaction, wherein signals are generated only at the focus of a laser beam. This has been proven to be a powerful tool for biomedical studies.[1–5] With signal generation supralinearly depending on the light intensity, nonlinear optical imaging techniques provide inherent three-dimensional (3-D) resolution[6] and reduced bulk photodamage, which is crucial for long-term imaging.[7] Nonlinear absorption imaging was recently reported by Warren's group for label-free *in vivo* imaging of microvasculature and oxygen level,[8] as well as label-free imaging and differentiation of eumelanin and pheomelanin[9] with endogenous contrast. Together with advantages such as inherent 3-D sectioning capabilities and micron-level resolution with high sensitivity,[10] this nonlinear absorption method could be used for detection of hypoxia and melanoma noninvasively and with high accuracy. Since nonlinear absorption imaging does not require chromophores with high-fluorescence quantum efficiency, a wider range of nonfluorescent probe molecules could be developed for functional imaging as well.

Using two-photon fluorescence (TPF), a limiting depth of 3 to 5 scattering mean-free-path L_s with optical powers of 600 mW has been reached.[11] For the case of nonlinear absorption imaging, the results reported were in transmission mode in turbid medium or epi-mode with an object not inside a turbid medium.[9] Nonlinear absorption imaging of objects embedded inside turbid media with backscattering detection has not yet been shown to date, to our knowledge. The ultimate penetration depth of this technique has not been reported in backscattering detection mode, either.

In previous studies of nonlinear absorption imaging, the two different wavelength signals required for pumping and probing were generated by two separate femtosecond laser systems. We demonstrate in this paper that a single laser can be used with a nonlinear optical fiber and optical filters to generate the required two signals, resulting in a significant simplification. With our simplified system, by imaging phantoms at different depths inside the turbid media, we further study for the first time the resolution and penetration depth limitation of the nonlinear absorption imaging method in the backscattering mode in a turbid medium.

In order to acquire images in turbid media, it is important to optimize the collection efficiency as much as possible.[12,13] The strong scattering environment[14] affects the fraction of detected photons. Monte Carlo is an established method to simulate photon propagation in scattering tissue.[15] It has been applied widely to analyze many kinds of imaging techniques, such as optical coherence tomography (OCT),[16] multiphoton

Address all correspondence to: Liping Cui, University of Rochester, The Institute of Optics, 275 Hutchinson Road, Rochester, New York 14620. Tel: 585-275-2323; Fax: 585-244-4936; E-mail: cui@optics.rochester.edu.

1083-3668/2010/15(2)/026004/6/$25.00 © 2010 SPIE

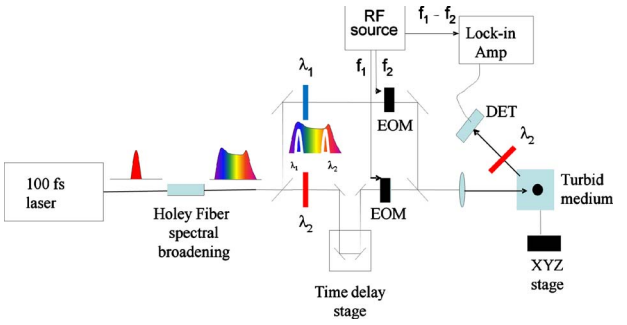

Fig. 1 Schemetic view of our single-laser, two-color, two-frequency experimental system. A 100-fs laser (Spectra-Physics Mai-Tai) beam is spectrally broadened in a holey fiber and selected with two notch interference filters in two separate beams. The signals are modulated at 980- and 1080-kHz frequencies with electro-optic modulators (EOMs) and are recombined and focused into a calibrated scattering cell on the sample. The nonlinear cross-product is detected at the difference frequency with a lock-in amplifier.

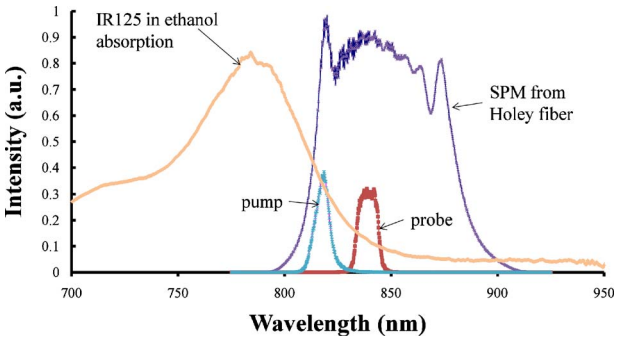

Fig. 2 Scheme of the spectra of SPM from holey fiber, absorption of IR125 in ethanol, and selected wavelengths.

fluorescence (MPF),[17,18] second-harmonic generation (SHG),[19] as well as third-harmonic generation,[20] etc. in turbid media. Here, a Monte Carlo–based simulation method (LightTools) is used to analyze the nonlinear absorption imaging in turbid media.

2 Experiment and Simulation Methods

2.1 *Imaging System*

The pump-probe technique has been used for decades as a standard nonlinear measurement tool for characterization of light-induced changes in materials' optical properties and relaxation dynamics of excited states.[21] The basic concept is that the transmission difference of the probe beam is measured with and without the application of a pump beam. The change in the probe beam signal is caused by the selective excitation of energy states within the molecules.[10,21]

Figure 1 shows the experimental setup. The laser has a repetition rate of 80 MHz, 100-fs pulse width, and wavelength tunable range from 780 nm to 920 nm. Laser pulses of 100-mW average power (pulse energies=1.25 nJ) are coupled into a holey fiber that is operated in normal-dispersion regime to generate low-noise, broadband, pure self-phase modulation (SPM).[22] The beam is then divided into two arms, in which we select two narrow wavelength bands at 800 nm and 840 nm with high-efficiency notch filters (Semrock FF01-800/12-25 & FF01-840/12-25), as shown in Fig. 1. One signal is delayed in the time domain by a computer-controlled translation stage, and these two wavelength signals are modulated at 980 and 1080 kHz, respectively, with electro-optic modulators (Thorlabs, EO-AM-NR-C1). The two arms are combined by a high-efficiency dichroic mirror collinearly and focused onto the object to be studied. The backscattered signals are collected by a large-area silicon PIN photodiode (EG&G SGD-200) in a 45-deg detection configuration and then detected with a lock-in amplifier at 100 kHz, which is the difference frequency. This high-frequency modulation technique provides lower noise and high-sensitivity detection.[23]

The pump and probe arms are collinearly focused onto the dye-filled capillary, which is put inside a 1-cm cuvette that contains the scattering solution. (Milk solution was used.) The cuvette is attached to a one-dimensional (1-D) translation stage to control the specific depth of the capillary tube relative to the front surface of the cuvette. At each controlled depth, the capillary tube is scanned in the plane vertical to the cuvette moving direction by a two-dimensional (2-D) stage to obtain 2-D images.

2.2 *Sample Calibration*

2.2.1 *Image object phantom*

Phantoms were prepared with IR125 dye in ethanol contained in capillary tubes with two different inner diameters (20 μm and 300 μm). The absorption spectrum of IR125 solution was measured with an Ocean Optics HR4000 spectrometer. The absorption spectrum peaks around 780 nm. We adjusted the laser center wavelength and self-phase modulation (SPM) spectrum out of the holey fiber to overlap with the absorption spectrum of the IR125. The pump and probe wavelengths were chosen from the overlap region between the absorption spectrum of IR125 in ethanol and the SPM laser spectrum out of the holey fiber, as shown in Fig. 2.

2.2.2 *Turbid medium*

Tissue phantoms or turbid media have been widely applied in the development of physical therapeutic or diagnostic imaging systems, including photodynamic therapy dosimetry, fluorescence imaging, OCT, and near-infrared (NIR) tomography.[24] Milk solution is commonly used, for instance, as a breast tissue phantom[25,26] or other tissue-like phantom.[24,27] In our experiments, we use it as a calibrated turbid medium to simulate a biological environment in order to understand the detection limits of this technique.

The milk solution's scattering mean-free-path L_s was determined by the transmission spectrum measured with an Ocean Optics HR4000 spectrometer. With transmission measured for the 10× diluted solution with 1-mm path length, the L_s of the undiluted solution could be calibrated, similar to one of the calibration methods in Ref. 13. By measuring the spectral transmission using a spectrophotometer, the scattering mean-free-path L_s was calculated by assuming that the absorption coefficient was small enough to be omitted so that transmission $T=\exp(-L/L_s)$, where L is the optical path of

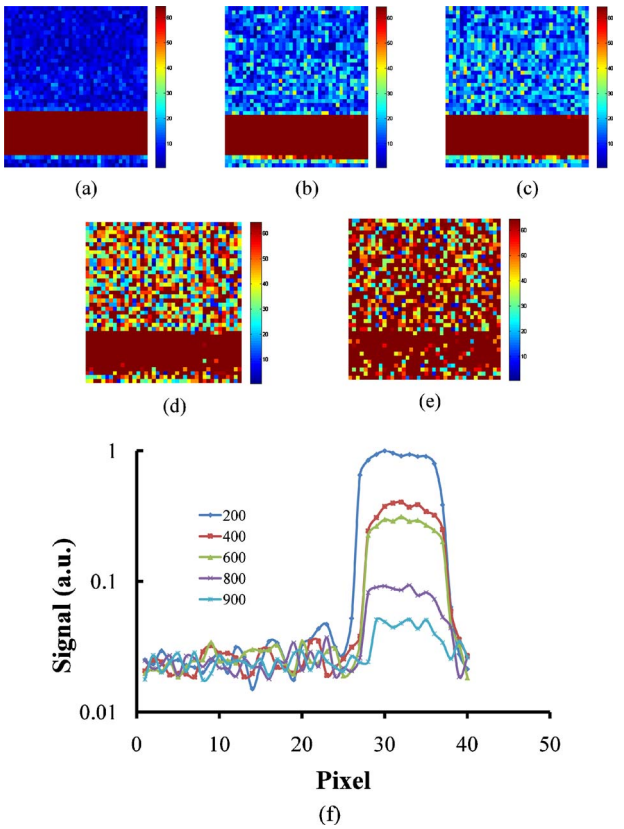

Fig. 3 Pump wavelength 800 nm; probe wavelength 840 nm. Nonlinear absorption images (30 μm/pixel, 40×40 pixels^2) of a 300-μm-diam capillary tube with 1-mW power per beam when the capillary tube is at (a) 200 μm, (b) 400 μm, (c) 600 μm, (d) 800 μm, and (e) 900 μm below the turbid medium surface. (f) Scan signal along the x axis at different depth (30 μm/pixel) with a logarithmic signal scale. The lock-in time constant was set at 100 ms.

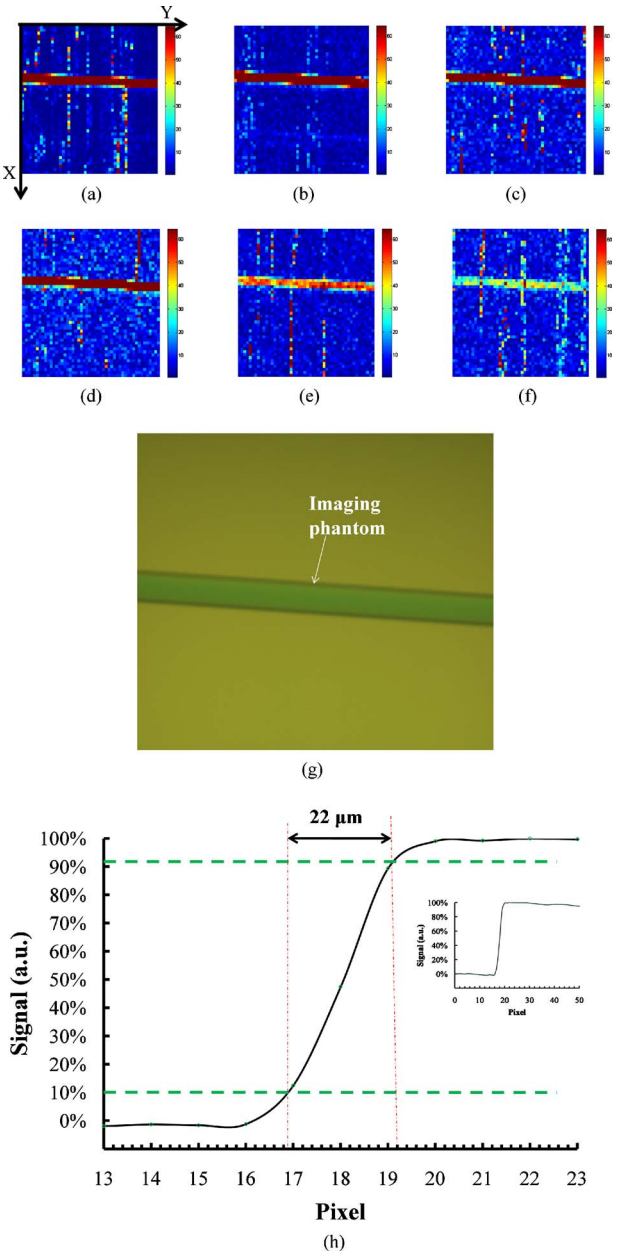

Fig. 4 Pump wavelength 800 nm; probe wavelength 840 nm. Nonlinear absorption images (500×500 microns) of 20-μm-diam capillary tube with 1-mW power at each beam when the capillary tube is at (a) 100 μm, (b) 200 μm, (c) 300 μm, (d) 400 μm, (e) 500 μm, and (f) 600 μm below the surface. (g) Bright-field image under microscope. (h) Zoomed integrated intensity signal along part of the x axis at 100 μm below the surface (10 μm/pixel), from which the width of the capillary tube is calibrated to be 22 μm. The inset in (h) is the integrated intensity along the whole x axis from the image result.

the scattering medium. This L_s result was consistent with that calculated by Mie theory and other methods.[13] In our studies, the milk solution for the 300-μm tube imaging was determined to have an L_s of 448 μm, with its 10× diluted solution having a transmission of 80% (optical density OD=0.97) for 1-mm optical path length; the L_s was 330 μm for milk solution in 25-μm-tube imaging with 74% (optical density OD =0.13) transmission for its 1-mm-thick 10× diluted solution.

2.3 *Monte Carlo–Based Simulation Method*

Light propagation in turbid media in this paper are simulated with a Monte Carlo–based method using LightTools software (Optical Research Associates, Inc.). Properties of the turbid media, such as mean-free-path length L_s, absorption coefficient, etc., are defined in the simulations according to the materials used.

3 Results and Discussion

3.1 *Backscattering Image Experimental Results*

We imaged a phantom of a single capillary tube (300-μm inner diameter) filled with IR125 in ethanol inside a calibrated milk solution (L_s=448 μm) at different focus depth to the front surface of the turbid medium. The wavelengths for the pump and probe signals are chosen to be 800 nm and 840 nm, respectively. Each beam contained about 1-mW average power. The detector was put close to the phantom with 45-deg angle to the incident laser beams as described earlier. The scanning signals were obtained at a depth from 200 μm to 900 μm below the surface [Figs. 3(a)–3(e)]. Red regions have the highest detected signals, and blue regions are the smallest signals. As expected, the detected signal-to-noise

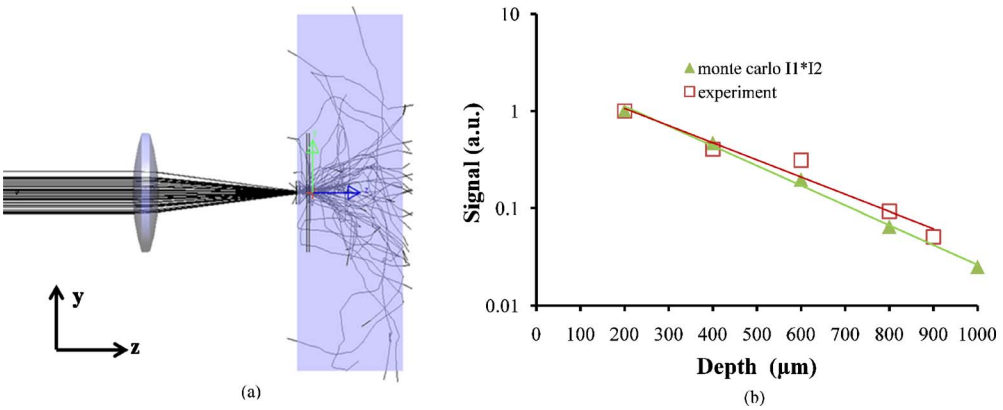

Fig. 5 Monte Carlo–based simulation for signal versus focus depth. (a) Side view of the simulation setup. (b) Comparison of experimental results with simulation ones: signals decrease exponentially at similar rate as the depth increases.

ratio (SNR) decreased as the imaging depth increased, as shown by the x-axis scan signal in Fig. 3. A limiting SNR ~ 1 was achieved at 900 μm, corresponding to more than 2 L_s of the turbid medium. The decreasing signal as a function of focus depth will be compared with simulation results in Sec. 3.2.

Next, a capillary tube with about 20-μm inner diameter filled with IR125 in ethanol was used as the object phantom imaged inside calibrated milk solution (L_s=330 μm). Each beam contained about 1-mW average power with the same wavelengths as before. The same detection configuration was utilized. Images obtained (500×500 μm^2 or 50×50 pixels^2) are shown in Figs. 4(a)–4(f) with capillary tube depth from 100 μm to 600 μm below the surface. The integrated intensity along the x axis at 100 μm below surface [Fig. 4(g)] was calculated to calibrate the transverse resolution of the image, which is defined by the distance of corresponding x positions at 10% and 90% of the maximum integrated intensity value. This distance was measured to be 22 ± 2 μm, which matches well with its actual width.

For the preceding experiments, the pump and probe beams were set to be linearly polarized. The backscattered light would be depolarized after propagation in a strongly scattering turbid medium,[28] and our detection method was independent of the polarization of the backscattering light.

Previously, Warren's group demonstrated the use of the nonlinear pump-probe technique for biological imaging.[8–10] We believe that this technique can be even more applicable to important biological imaging problems if it can be made to work efficiently in backscattering mode. The current phantom experiments help us to understand the limitations of the backscattering mode detection.

3.2 *Analysis by Monte Carlo–Based Simulation*

To understand and analyze the nonlinear absorption signal's propagation in turbid media for the case of a backscattering detection, we applied a Monte Carlo–based method using the software LightTools. Turbid media having an L_s of 448 μm was held inside a 1-cm cuvette.

For our first simulation, 1,000,000 rays were focused into the turbid medium by a singlet with a focus length of $\sim$1.5 cm, as illustrated in Fig. 5(a). (Only 50 rays are shown of the 1,000,000 used in the calculation.) A dummy surface was inserted inside the turbid medium at the focus point so that the distribution of rays at the focus point surface could be measured.

By moving the cuvette along the z axis, the focus depth relative to the front surface of the turbid medium was changed accordingly. The number of rays incident at the focus point for focus depth varying from 200 μm to 1 mm below the surface had been obtained by simulation. The simulation was repeated for wavelengths 800 nm (I_1) and 840 nm (I_2), the wavelengths used for the pump and probe signals in the experiment. The product of the two focused intensities for the two wavelengths at corresponding depths was normalized to compare with the normalized x-axis scan peak values of the 300-μm capillary tube images [Fig. 3(f)] obtained from our experiment, where the turbid medium had the same L_s length. This is appropriate since the nonlinear absorption signal is generated only by the product of the two focused intensities.

By plotting the nonlinear absorption image signal values as a function of different focus depth, both our experimental data and our simulation data could be fit well with similar exponential curves [Fig. 5(b)]. The experimental curve is fit with $y=2.4\exp(-x/250)$, and the simulation data is fit with $y=2.8\exp(-x/200)$, where x is the depth of the focus with units of microns. The variance of the two curves is within a reasonable range, which might be caused by the errors of experimental measurement.

A second simulation is done to estimate the collection efficiency of our 45-deg detection method. A detector was put at a 45-deg angle to the cuvette, as shown in the top view in Fig. 6(a). 1,000,000 rays were generated at the focus point with forward directions falling inside a 5-deg cone, which corresponds to the NA of the focus lens. The focus point was assumed to be 1 mm below the turbid medium surface. The backscattered signal reemitted to the detector was calculated by the ratio of power integrated to the initial total signal power generated at the focus point as a function of the radius of the detector.

Figure 6(b) shows that as the radius of the detector increases, more signals are collected by the detector, as expected, but only about 2% of the signal photons are collected on a 5-mm-radius detector. We are investigating multiple-

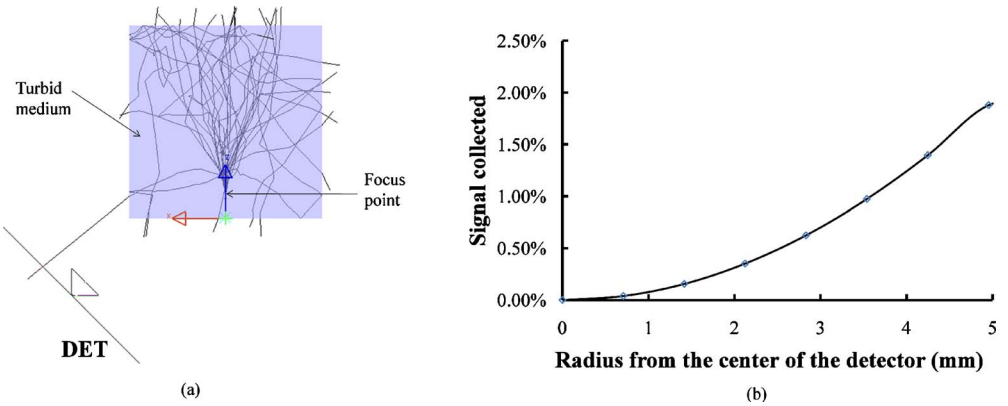

Fig. 6 Monte Carlo-based simulation for detection process. (a) Top view of the simulation setup (only 30 rays visible). (b) Simulation results of the percentages of integrated power on the detector to the total signal power as a function of radius to the center of the detector.

detector schemes that can increase this fraction; however, clearly our results show that backscattering mode detection does indeed work with moderate pump and probe signal powers, benefiting from the high-frequency detection technique.

4 Conclusions

We have demonstrated the use of a holey fiber SPM generator-based, two-color, two-frequency nonlinear absorption imaging system for imaging in backscattering mode in turbid media. The approach is simpler than two-laser schemes, has a large potential wavelength coverage range, and avoids the spatial laser beam mismatching compared to previous reports. Image resolution of $\sim$20 μm has been demonstrated by imaging a 20-μm tube filled with IR125 in ethanol up to a depth of 600 μm. Imaging depth of 900 μm at SNR $\sim$1 was achieved with 1 mW per beam in a calibrated scattering solution by imaging a 300-μm-diam capillary tube phantom filled with IR125 dye in ethanol. With higher powers, we expect to be able to achieve higher penetration depths.

A Monte Carlo–based method is used for the first time to simulate and analyze the nonlinear absorption imaging in turbid media. The results show that the nonlinear signal decreases exponentially as the focus depth increases, and the decreasing rate matches the experimental results well. With the use of the simulation, we show that 2% collection coefficient is typically achieved with our detection method. With all the previous work in forward-scattering mode, adding the ability to image in backscattering mode in a turbid medium means that this technique could be a promising method for clinical practice.

We are currently optimizing the detection and investigating applications in biological tissues, as well as making a one-to-one comparison with two-photon fluorescence–based imaging. These will be reported elsewhere.

Acknowledgments

The authors wish to thank Prof. Andrew Berger at The Institute of Optics at the University of Rochester for fruitful discussions. We are also grateful to Richard Bauserman for his technical assistant with capillary tube fabrication.

References

1. W. R. Zipfel, R. M. Williams, and W. W. Webb, "Nonlinear magic: multiphoton microscopy in the biosciences," *Nat. Biotechnol.* **21**, 1369–1377 (2003).
2. F. Helmchen and W. Denk, "New developments in multiphoton microscopy," *Curr. Opin. Neurobiol.* **12**, 593–601 (2002).
3. E. Brown, T. McKee, E. diTomaso, A. Pluen, B. Seed, Y. Boucher, and R. K. Jain, "Dynamic imaging of collagen and its modulation in tumors *in vivo* using second-harmonic generation," *Nat. Med.* **9**, 796–800 (2003).
4. C. L. Evans, E. O. Potma, M. Puoris'haag, D. Cote, C. P. Lin, and X. S. Xie, "Chemical imaging of tissue *in vivo* with video-rate coherent anti-Stokes Raman scattering microscopy," *Proc. Natl. Acad. Sci. U.S.A.* **102**, 16807–16812 (2005).
5. F. Helmchen and W. Denk, "Deep tissue two-photon microscopy," *Nat. Methods* **2**, 932–940 (2005).
6. W. Denk, J. H. Strickler, and W. W. Webb, "2-photon laser scanning fluorescence microscopy," *Science* **248**, 73–76 (1990).
7. J. M. Squirrell, D. L. Wokosin, J. G. White, and B. D. Bavister, "Long-term two-photon fluorescence imaging of mammalian embryos without compromising viability," *Nat. Biotechnol.* **17**, 763–767 (1999).
8. D. Fu, T. E. Matthews, T. Ye, I. R. Piletic, and W. S. Warren, "Label-free *in vivo* optical imaging of microvasculature and oxygenation level," *J. Biomed. Opt.* **13**, 040503 (2008).
9. D. Fu, T. Ye, T. E. Matthews, J. Grichnik, L. Hong, J. D. Simon, and W. S. Warren, "Probing skin pigmentation changes with transient absorption imaging of eumelanin and pheomelanin," *J. Biomed. Opt.* **13**, 054036 (2008).
10. D. Fu, T. Ye, T. E. Matthews, B. J. Chen, G. Yurtserver, and W. S. Warren, "High-resolution *in vivo* imaging of blood vessels without labeling," *Opt. Lett.* **32**, 2641–2643 (2007).
11. P. Theer, M. T. Hasan, and W. Denk, "Two-photon imaging to a depth of 1000 microm in living brains by use of a Ti:Al2O3 regenerative amplifier," *Opt. Lett.* **28**, 1022–1024 (2003).
12. M. Oheim, E. Beaurepaire, E. Chaigneau, J. Mertz, and S. Charpak, "Two-photon microscopy in brain tissue: parameters influencing the imaging depth," *J. Neurosci. Methods* **111**, 29–37 (2001).
13. P. Theer and W. Denk, "On the fundamental imaging-depth limit in two-photon microscopy," *J. Opt. Soc. Am. A* **23**, 3139–3149 (2006).
14. W. F. Cheong, S. A. Prahl, and A. J. Welch, "A review of the optical-properties of biological tissues," *IEEE J. Quantum Electron.* **26**, 2166–2185 (1990).
15. L. Wang, S. L. Jacques, and L. Zheng, "MCML—Monte Carlo modeling of light transport in multi-layered tissues," *Comput. Methods Programs Biomed.* **47**, 131–146 (1995).
16. Q. Lu, X. S. Gan, M. Gu, and Q. M. Luo, "Monte Carlo modeling of optical coherence tomography imaging through turbid media," *Appl. Opt.* **43**, 1628–1637 (2004).
17. C. Wang, L. L. Qiao, Z. L. Mao, Y. Cheng, and Z. Z. Xu, "Reduced deep-tissue image degradation in three-dimensional multiphoton microscopy with concentric two-color two-photon fluorescence excita-

tion," *J. Opt. Soc. Am. B* **25**, 976–982 (2008).
18. X. Y. Deng, X. S. Gan, and M. Gu, "Monte Carlo simulation of multiphoton fluorescence microscopic imaging through inhomogeneous tissue-like turbid media," *J. Biomed. Opt.* **8**, 440–449 (2003).
19. X. Y. Deng, X. J. Wang, H. P. Liu, Z. F. Zhuang, and Z. Y. Guo, "Simulation study of second-harmonic microscopic imaging signals through tissue-like turbid media," *J. Biomed. Opt.* **11**, 024013 (2006).
20. D. Debarre, N. Olivier, and E. Beaurepaire, "Signal epidetection in third-harmonic generation microscopy of turbid media," *Opt. Express* **15**, 8913–8924 (2007).
21. C. H. Brito Cruz, R. L. Fork, W. H. Knox, and C. V. Shank, "Spectral hole burning in large molecules probed with 10-fs optical pulses," *Chem. Phys. Lett.* **132**, 341–344 (1986).
22. F. Lu and W. H. Knox, "Generation of a broadband continuum with high spectral coherence in tapered single-mode optical fibers," *Opt. Express* **12**, 347–353 (2004).
23. C. W. Freudiger, W. Min, B. G. Saar, S. Lu, G. R. Holtom, C. He, J. C. Tsai, J. X. Kang, and X. S. Xie, "Label-free biomedical imaging with high sensitivity by stimulated Raman scattering microscopy," *Science* **322**, 1857–1861 (2008).
24. B. W. Pogue and M. S. Patterson, "Review of tissue simulating phantoms for optical spectroscopy, imaging and dosimetry," *J. Biomed. Opt.* **11**, 041102 (2006).
25. B. Drexler, J. L. Davis, and G. Schofield, "Diaphanography in the diagnosis of breast cancer," *Radiology* **157**, 41–44 (1985).
26. T. D. Khokhlova, I. M. Pelivanov, V. V. Kozhushko, A. N. Zharinov, V. S. Solomatin, and A. A. Karabutov, "Optoacoustic imaging of absorbing objects in a turbid medium: ultimate sensitivity and application to breast cancer diagnostics," *Appl. Opt.* **46**, 262–272 (2007).
27. G. Mitic, J. Kolzer, J. Otto, E. Plies, G. Solkner, and W. Zinth, "Time-gated transillumination of biological tissues and tissue-like phantoms," *Appl. Opt.* **33**, 6699–6710 (1994).
28. V. Sankaran, M. J. Everett, D. J. Maitland, and J. T. Walsh, "Comparison of polarized-light propagation in biological tissue and phantoms," *Opt. Lett.* **24**, 1044–1046 (1999).